into account. For an unpolarized incident beam, the usual case in neutron powder diffraction, it is a useful consequence of the triple vector product that the magnetic scattering depends on the sine of the angle that the scattering vector makes with the magnetic moment on the scattering atom (see Section 2.3.4 and Chapter 7 in Kisi & Howard, 2008). The extent of the unpaired electron distribution (usually outer electrons) implies that the scattering diminishes as a function of Q, an effect that can be described by a magnetic form factor. For a well defined direction for the magnetic moment $\mathbf{M}$, and with a distribution of moment that can be described by a normalized scalar $m(\mathbf{r})$, the form factor as a function of the scattering vector $\mathbf{h}$ [defined in equation (1.1.17) in Chapter 1.1][6] is the Fourier transform of $m(\mathbf{r})$,

$$f(\mathbf{h}) = \int m(\mathbf{r}) \exp(2\pi i \mathbf{h} \cdot \mathbf{r})\, \mathrm{d}\mathbf{r},$$

where $m(\mathbf{r})$ can comprise both spin and orbital contributions [Section 6.1.2 of Volume C (Brown, 2006*a*)]. The tabulated form factors are based on the assumption that the electron distributions are spherically symmetric, so that $m(\mathbf{r}) = m(r) = U^2(r)$, where $U(r)$ is the radial part of the wave function for the unpaired electron. In the expansion of the plane-wave function $\exp(2\pi i \mathbf{h} \cdot \mathbf{r})$ in terms of spherical Bessel functions, we find that the leading term is just the zeroth-order spherical Bessel function $j_0(2\pi hr)$ with a Fourier transform

$$\langle j_0(h) \rangle = 4\pi \int_0^\infty U^2(r) j_0(2\pi hr) r^2\, \mathrm{d}r.$$

This quantity is inherently normalized to unity at $h = 0$, and may suffice to describe the form factor for spherical spin-only cases. In other cases it may be necessary to include additional terms in the expansion, and these have Fourier transforms of the form

$$\langle j_l(h) \rangle = 4\pi \int_0^\infty U^2(r) j_l(2\pi hr) r^2\, \mathrm{d}r$$

with l even; these terms are zero at $h = 0$ (Brown, 2006*a*). In practice these quantities are evaluated using theoretical calculations of the radial distribution functions for the unpaired electrons [Section 4.4.5 of Volume C (Brown, 2006*b*)].

Form factors can be obtained from data tabulated in Section 4.4.5 of Volume C (Brown, 2006*b*). Data are available for elements and ions in the 3*d*- and 4*d*-block transition series, for rare-earth ions and for actinide ions. These data are provided by way of the coefficients of analytical approximations to $\langle j_l(h) \rangle$, the analytical approximations being

$$\langle j_0(s) \rangle = A \exp\left(-as^2\right) + B \exp\left(-bs^2\right) + C \exp\left(-cs^2\right) + D$$

and for $l \neq 0$

$$\langle j_l(s) \rangle = s^2 \left[A \exp\left(-as^2\right) + B \exp\left(-bs^2\right) + C \exp\left(-cs^2\right) + D\right],$$

where $s = h/2$ in Å^{-1}. These approximations, with the appropriate coefficients, are expected to be coded in to any computer program purporting to analyse magnetic structures. Although the tabulated form factors are based on theoretical wave functions, it is worth noting that the incoherent scattering from an ideally disordered (*i.e.*, paramagnetic) magnetic system will display the magnetic form factor directly.

It is often convenient to define a (Q-dependent) magnetic scattering length

$$p = \left(\frac{e^2\gamma}{2m_e c^2}\right) gJf,$$

where m_e and e are the mass and charge of the electron, γ ($= \mu_n$) is the magnetic moment of the neutron, c is the speed of light, J is the total angular momentum quantum number, and g is the Landé splitting factor given in terms of the spin S, orbital angular momentum L, and total angular momentum quantum numbers by

$$g = 1 + \frac{J(J+1) + S(S+1) - L(L+1)}{2J(J+1)}.$$

For the spin-only case, $L = 0$, $J = S$, so $g = 2$. The differential magnetic scattering cross section per atom is then given by q^2p^2 where $|q| = \sin\alpha$, α being the angle between the scattering vector and the direction of the magnetic moment. This geometrical factor is very important, since it can help in the determination of the orientation of the moment of interest; there is no signal, for example, when the moment is parallel to the scattering vector. Further discussion appears in Chapters 2 (Section 2.3.4) and 7 in Kisi & Howard (2008).

2.3.2.6. *Structure factors*

The locations of the Bragg peaks for neutrons are calculated as they are for X-rays[7] (Section 1.1.2), and the intensities of these peaks are determined by a structure factor, which in the nuclear case is [*cf.* Chapter 1.1, equation (1.1.56)]

$$F_{hkl}^{\text{nuc}} = \sum_{i=1}^{m} b_i T_i \exp(2\pi i \mathbf{h} \cdot \mathbf{u}_i), \tag{2.3.7}$$

where b_i here denotes the coherent scattering length, T_i has been introduced to represent the effect of atomic displacements (thermal or otherwise, see Section 2.4.1 in Kisi & Howard, 2008), $\mathbf{h}$ is the scattering vector for the hkl reflection, and the vectors $\mathbf{u}_i$ represent the positions of the m atoms in the unit cell.

For coherent magnetic scattering, the structure factor reads

$$F_{hkl}^{\text{mag}} = \sum_{i=1}^{m} p_i \mathbf{q}_i T_i \exp(2\pi i \mathbf{h} \cdot \mathbf{u}_i), \tag{2.3.8}$$

where p_i is the magnetic scattering length. The vector $\mathbf{q}_i$ is the 'magnetic interaction vector' and is defined by a triple vector product (Section 2.3.4 in Kisi & Howard, 2008), and has modulus $\sin\alpha$ as already mentioned. In this case the sum needs to be taken over the magnetic atoms only.

As expected by analogy with the X-ray case, the intensity of purely nuclear scattering is proportional to the square of the modulus of the structure factor $|F_{hkl}^{\text{nuc}}|^2$. In the simplest case of a collinear magnetic structure and an unpolarized incident neutron beam, the intensity contributed by the magnetic scattering is proportional to $|F_{hkl}^{\text{mag}}|^2$, and the nuclear and magnetic contributions are additive.

2.3.3. Neutron sources

2.3.3.1. *The earliest neutron sources*

The earliest neutron source appears to have been beryllium irradiated with α-particles (helium nuclei), as emitted for example by polonium or radon. First described as 'beryllium radiation', the radiation from a Po/Be source was identified by

[6] To reiterate, $\mathbf{h} = \mathbf{s} - \mathbf{s}_0$, where $\mathbf{s}_0$ and $\mathbf{s}$ are vectors, each of magnitude $1/\lambda$, defining the incident and scattered beams. Note that $\mathbf{Q} = 2\pi\mathbf{h}$.

[7] The nuclear unit cell is expected to coincide with the X-ray unit cell, but the magnetic unit cell may be larger. So, although the methods of calculation are the same, the larger magnetic cell may give rise to additional (magnetic) Bragg peaks.

Chadwick (1932) as comprising neutrons:

$$^{4}_{2}\mathrm{He} + ^{9}_{4}\mathrm{Be} \rightarrow ^{12}_{6}\mathrm{C} + ^{1}_{0}\mathrm{n}.$$

It was soon found (Szilard & Chalmers, 1934) that the disintegration of beryllium under irradiation by the γ-rays from radium also led to the release of neutrons; this represented an alternative neutron source. The first demonstrations of the diffraction of neutrons (Mitchell & Powers, 1936; von Halban & Preiswerk, 1936) made use of Rn/Be sources, analogous to Chadwick's Po/Be source. These were now surrounded by paraffin to reduce the energy ('moderate') and hence increase the de Broglie wavelength of the neutrons, and so provide a reasonable match to the atomic spacings in the crystalline samples; in the Mitchell & Powers' demonstration the reflection of neutrons of estimated wavelength 1.6 Å from (100) planes in large single crystals of MgO, the separation of these planes being 4.2 Å, showed a dependence on crystal orientation that was indicative of Bragg reflection. The intensities available from these sources, however, were not sufficient to allow the observation of diffraction from polycrystalline (powder) samples.

A source based on the bombardment of Be by cyclotron-accelerated MeV deuterons (nuclei of deuterium)

$$^{2}_{1}\mathrm{H} + ^{9}_{4}\mathrm{Be} \rightarrow ^{10}_{5}\mathrm{B} + ^{1}_{0}\mathrm{n}$$

was also employed in early work, notably by Alvarez & Bloch (1940) in their determination of the neutron magnetic moment.

The further development of neutron diffraction, and indeed the first observation of neutron powder diffraction, awaited the development of much more intense neutron sources; the first suitably intense neutron sources were nuclear reactors. The neutron-induced fission of uranium isotope $^{235}_{92}$U was observed in 1938 and reported early in 1939 (Hahn & Strassmann, 1939; Meitner & Frisch, 1939; Anderson *et al.*, 1939). By this time Fermi and his co-workers (Fermi, Amaldi, D'Agostino *et al.*, 1934; Fermi, Amaldi, Pontecorvo *et al.*, 1934) had already carried out studies on neutron activation, in the course of which they found that neutrons could be moderated by hydrogenous materials, providing 'slow' neutrons for which the activation cross sections were enhanced. Once it was established that the neutron-induced fission of a $^{235}_{92}$U nucleus also led to the release of ~2–3 'fast' neutrons plus energy (von Halban *et al.*, 1939; Zinn & Szilard, 1939), then a self-sustaining 'chain reaction' based on the fission of $^{235}_{92}$U by a slow neutron, the slowing in a moderator of the several fast neutrons released, followed by the slow-neutron-induced fission of additional $^{235}_{92}$U nuclei, became a realistic possibility. The translation of this possibility into reality was given great impetus by the military potential of the chain reaction; the reader is referred to Mason *et al.* (2013) for the history of this development. The first self-sustaining chain reaction took place in Chicago Pile 1 (CP-1) on 2 December 1942. CP-1 made use of uranium oxide mixed with some metallic uranium as fuel, high-purity graphite as the neutron moderator and rods of neutron-absorbing cadmium for control. CP-1 was located on a squash court under the spectator stand at a sports field at the University of Chicago; remarkably, its construction took less than a month. In November 1943, an essentially scaled up version of this reactor, the X-10 pile (also known as the Oak Ridge Graphite Reactor) achieved criticality. The fuel was now metallic uranium, and the greater power (1 MW as compared with the 200 W of CP-1) necessitated an air cooling system; the neutron flux[8] was a creditable 10^{12} n cm^{-2} s^{-1} and the main purpose was the production of plutonium. May 1944 saw the completion of yet another reactor, Chicago Pile 3 (CP-3), outside Chicago at the site of the present Argonne laboratories. This was a 300 kW reactor, using natural uranium fuel, with heavy water serving as both moderator and coolant; this also provided a flux of 10^{12} n cm^{-2} s^{-1}.

Early diffraction experiments using reactor neutrons were carried out 'in the wings of the Manhattan project' (Mason *et al.*, 2013). Evidently, Wollan & Borst (1945) obtained rocking curves when collimated thermal neutrons from X-10 were beamed onto single crystals of gypsum and rocksalt, while Zinn was able to reflect neutrons from a calcite crystal [see, for example, the post-war publication by Zinn (1947)]; much of the wartime interest was in using these crystals for neutron spectrometry. However, the potential use of these copious sources of neutrons was recognized, so by the early months of 1946 (according to Shull, 1995) the first neutron powder-diffraction patterns, from polycrystalline NaCl and from light and heavy water, had been recorded. Wollan and co-workers (Wollan & Shull, 1948; Shull *et al.*, 1948) published a number of these early diffraction patterns, along with a schematic of the diffractometer employed.

Although accelerator-based neutron sources had been around as early as 1940 (see above), the development of such sources, at least for diffraction applications, proceeded at a relatively slower pace. Indeed, it was not until 1968 that the first reports of neutron powder diffraction using accelerator-based sources appeared in the literature (Moore *et al.*, 1968; Kimura *et al.*, 1969; Day & Sinclair, 1969). All this work involved the use of linear electron accelerators (LINACs) delivering pulses of ~150 MeV electrons onto a heavy-metal target; the deceleration results in *Bremsstrahlung* radiation (photons) of sufficient energy to bring about the release of neutrons from the target. These fast neutrons were moderated, and the result was a pulsed source of thermal neutrons. Diffraction patterns were recorded by time-of-flight methods which had already been developed on reactor sources (Buras & Leciejewicz, 1964).

It may be helpful to describe one of these experiments in more detail (Kimura *et al.*, 1969). A tungsten target immersed in water was bombarded by 2.5 μs pulses of 250 MeV electrons from the Tohoku LINAC; the water, which served as a moderator, was also 'poisoned' by the addition of neutron-absorbing boric acid. The thermal neutron pulses were of 30–50 μs duration. It is a fundamental problem that the time taken to moderate the fast neutrons produced at an accelerator-based source degrades the time structure, and the addition of boron here was one method to counteract this effect. Kimura *et al.* presented a selection of time-of-flight diffraction patterns, from Al at different temperatures, as well as from Si, Ni, ZnO, $CaFe_2O_4$ and α-Fe_2O_3.

The next generation of accelerator-based sources were spallation sources, based on the breaking up of heavy target elements by bombardment with 10–1000 MeV protons; up to ~30 neutrons are ejected in each spallation event; such sources can be operated in either a pulsed mode or continuously. The first spallation sources were ZING-P (100 nA of 300 MeV protons, pulsed at 30 Hz, target Pb, moderator polyethylene) and ZING-P′ (3 μA of 500 MeV protons, 30 Hz, target W/natural U, moderator polyethylene/liquid hydrogen), both at the Argonne National Laboratory (Carpenter, 1977), and at the TRIUMF laboratory (400 μA of 500 MeV protons, steady, target liquid Pb/Bi, moderator light/heavy water) in Vancouver. The KENS facility (operational from 1980 to 2005, 9 μA of 500 MeV protons, 20 Hz, target W, moderator solid methane/ice) in Tsukuba, Japan, and

[8] The powers and fluxes given here are taken from a presentation by T. E. Mason at the Bragg Symposium, Adelaide, 6 December 2012.

the Intense Pulsed Neutron Source (IPNS) at the Argonne National Laboratory (operational from 1981 to 2008, 15 μA of 450 MeV protons, 30 Hz, target depleted U, moderator solid/liquid methane) are both worthy of mention for their work on techniques and applications at pulsed neutron sources; notable are contributions from IPNS on the subjects of high-temperature superconductors (Jorgensen *et al.*, 1987) and colossal magnetoresistance (Radaelli *et al.*, 1997).

The specifications and performance of modern currently operating spallation neutron sources will be presented in Section 2.3.3.3.

2.3.3.2. *Fission reactors for neutron-beam research*

Reactors used for neutron-beam research all rely on the fissile uranium isotope[9] $^{235}_{92}$U. This constitutes only about 0.7% of natural uranium; however, enrichment in this isotope is possible. A representative fission event would be

$$^{1}_{0}\mathrm{n} + {}^{235}_{92}\mathrm{U} \rightarrow {}^{236}_{92}\mathrm{U} \rightarrow {}^{141}_{56}\mathrm{Ba} + {}^{92}_{36}\mathrm{Kr} + 3{}^{1}_{0}\mathrm{n} + 170\ \mathrm{MeV}.$$

This equation indicates that a neutron of thermal energy is captured by ^{235}U to form ^{236}U in an unstable state, and in the majority of cases (88%) this breaks up almost instantly to yield fission products of intermediate mass, fast neutrons and energy. The unstable ^{236}U can break up in many different ways – there are usually products of intermediate but unequal masses, with masses distributed around 95 and 135 (Burcham, 1979), with the release of usually 2 or 3 neutrons (average 2.5; one of these neutrons is needed to initiate the next fission event), and of different amounts of energy (average around 200 MeV). As explained in Section 2.3.3.1, a chain reaction becomes possible if the fast neutrons released in the fission process are moderated to thermal energies so that they can be captured by another ^{235}U nucleus. Neutrons will lose energy most rapidly through collisions with nuclei of mass equal to the neutron mass, namely nuclei of hydrogen atoms, but collisions with other light nuclei are also quite effective. Hydrogenous substances are evidently useful, and water would seem ideal; however, there is some absorption of neutrons in water, so in some reactors, heavy water (D_2O, where D is $^{2}_{1}$H) is used since, as can be seen from the absorption cross sections (Table 2.3.2), thermal neutron capture in D is orders of magnitude less than for H. It has not been possible to achieve a self-sustaining chain reaction using natural uranium and light water as a moderator – for this reason uranium fuel enriched in ^{235}U and/or heavy-water moderators are in use. Adjacent to the reactor core is a so-called reflector, which is simply in place to moderate neutrons and prevent their premature escape. The energy released in the fission process ends up as heat, which must be dissipated (or used), so cooling is required – where light or heavy water is used as the moderator it can also serve as the coolant. Control rods are also essential – these are rods containing highly neutron absorbing materials, such as boron, cadmium or hafnium, which can be inserted into or withdrawn from the reactor to increase, maintain or reduce the thermal neutron flux as required. These control rods provide the means for reactor shutdown.

The neutrons in a reactor core range from the fast neutrons (~1 MeV) released in the fission process, through epithermal neutrons (in the range eV to keV), which are neutrons in the process of slowing down, to thermal neutrons (~25 meV), which are neutrons in equilibrium with the moderator (see Carlile, 2003). Evidently, for sustaining the chain reaction and for providing neutrons for diffraction instruments, the thermal neutrons are of the greatest interest. Neutrons in thermal equilibrium with the moderator have a Maxwellian distribution of energies, such that the number of neutrons with energies between E and $E + \mathrm{d}E$ is given by $N(E)\,\mathrm{d}E$, where

$$N(E) = \frac{2\pi N_0}{(\pi k_B T)^{3/2}}(E)^{1/2}\exp(-E/k_B T). \qquad (2.3.9)$$

Here N_0 is the total number of neutrons, T is the temperature (in kelvin) of the moderator, and k_B is Boltzmann's constant. The neutron flux is the product of the neutron density with the neutron speed, so the energy dependence of the flux distribution takes the form

$$\varphi(E) = \varphi_0 \frac{E}{(k_B T)^{3/2}}\exp(-E/k_B T). \qquad (2.3.10)$$

This distribution takes its peak value at $E = k_B T$; for a temperature of 293 K, this leads to a peak in the flux distribution at 25.2 meV (*cf.* Section 2.3.1). In the diffraction context the wavelength dependence of the flux is of more interest. Making use of the relationships $E = h^2/2m\lambda^2$ and $\mathrm{d}E/\mathrm{d}\lambda = -h^2/m\lambda^3$, we find that the variation of flux with wavelength can be described by $\varphi(\lambda)\,\mathrm{d}\lambda$, where

$$\varphi(\lambda) \propto \lambda^{-5}\exp(-h^2/2m\lambda^2 k_B T). \qquad (2.3.11)$$

This distribution peaks at $\lambda = h/(5mk_B T)^{1/2}$; at 293 K the peak in this wavelength distribution is at 1.15 Å. For some applications of neutron diffraction it may be desirable to have a greater neutron flux at shorter or longer wavelengths; as indicated in Fig. 2.3.5 this can be achieved by cooling or heating strategically placed special moderators.

As one specific example of a research reactor, we consider the NBSR located at the National Institute of Standards and Technology, Gaithersburg, USA. This reactor uses highly enriched (93% ^{235}U) uranium in U_3O_8-Al as fuel, and heavy water as moderator and coolant. The thermal neutron flux in this reactor is 4×10^{14} n cm^{-2} s^{-1}. It uses four cadmium control blades. An early plan view of this reactor and a cutaway view of the core assembly

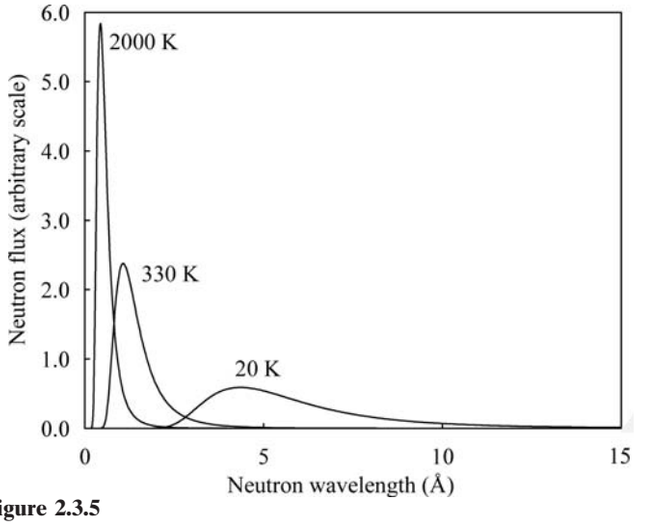

Figure 2.3.5
The Maxwellian distribution of neutron wavelengths produced within moderators at different temperatures. Reproduced from Kisi & Howard (2008) by permission of Oxford University Press.

[9] Bombardment with >1 MeV neutrons can cause the fission of the predominant uranium isotope ^{238}U; however, there are too few neutrons at these energies to support a chain reaction based on this isotope.

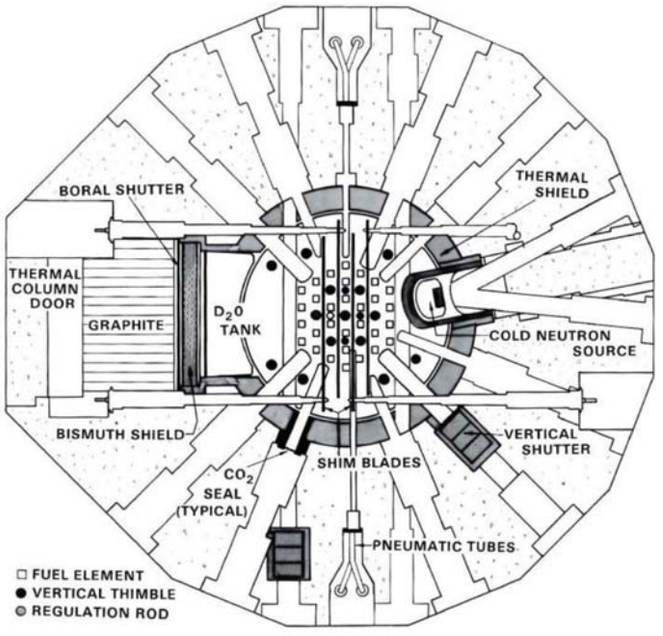

Figure 2.3.6
The NBSR at the National Institute of Standards and Technology Center for Neutron Research. Part (*a*) is a plan view (reproduced from Rush & Cappelletti, 2011) while (*b*) is a recent cutaway view of the reactor core showing the liquid-hydrogen cold source on the right-hand side.

are shown in Fig. 2.3.6. Note the presence of numerous beam tubes that allow neutrons to be taken out from the vicinity of the reactor core. This view of the NBSR (Fig. 2.3.6*a*) shows provision for a cold neutron source, and for beam tubes to transport cold neutrons to experiments, but it was years before any cold neutron source was installed. The first cold source, installed in 1987, was frozen heavy water; this was replaced in 1995 by a liquid-hydrogen cold source, and that was upgraded in turn in 2003. The NBSR first went critical in December 1967; the history of its subsequent development and use in neutron-beam research has been recounted by Rush & Cappelletti (2011).

The HFR at the Institut Laue–Langevin (ILL), considered to be the premier source for reactor-based neutron-beam research, serves as our second example. It too uses highly enriched uranium, here in a single centrally located U_3Al_x-Al fuel element, and it relies on heavy water for moderator and coolant. It operates at 58 MW and the thermal neutron flux is 1.5 $\times$

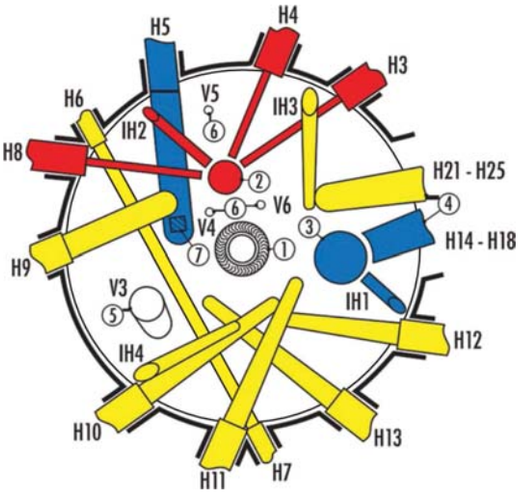

Figure 2.3.7
Schematic diagram of the HFR operated by the Institut Laue–Langevin in Grenoble, France. It has a compact core – the beam tubes avoid viewing the central core in favour of the surrounding moderator. This reactor also features hot (red) and cold (blue) sources. (Diagram reproduced with permission from the ILL from The Yellow Book 2008, https://www.ill.eu/fileadmin/users_files/Other_Sites/Yellow-Book2008CDRom/index.htm.)

10^{15} n cm^{-2} s^{-1}. The reactor incorporates two liquid-deuterium cold sources, operating at 20 K, and a graphite hot source operating at 2000 K. In the HFR, being of modern design and purpose-built for neutron-beam research, the beam tubes do not view the core directly, but are 'tangential' to it (Fig. 2.3.7); this reduces the unwelcome fast-neutron component of the emerging beams. The HFR achieved criticality in July 1971. More details on this reactor can be found in the 'Yellow Book' which is maintained on the ILL web site, https://www.ill.eu.

From the opening paragraph of this section, it might be concluded that the more heavy water deployed, and the more highly is the uranium enriched in the fissile isotope ^{235}U, the greater the neutron fluxes that can be obtained. This conclusion would be correct, but concerns about nuclear proliferation have brought a shift to the use of low-enrichment uranium (LEU) in which the ^{235}U is enriched to less than 20%; however, in some reactors highly enriched uranium (HEU) with enrichment levels greater than 90% remains in use. Table 2.3.3 gives pertinent details on a number of research reactors important for neutron diffraction. Additional reactors are listed by Kisi & Howard (2008) in their Table 3.1, and a complete listing is available from the International Atomic Energy Agency Research Reactor Database (IAEA RRDB, https://nucleus.iaea.org/RRDB/RR/ReactorSearch.aspx).

2.3.3.3. *Spallation neutron sources*

The bombardment of heavy-element nuclei by high-energy protons, *i.e.* protons in the energy range 100 MeV to GeV, causes the nuclei to break up with the release of large numbers of neutrons. The word 'spallation' might suggest that neutrons are simply being chipped off the target nucleus, and indeed neutrons can be ejected by protons in a direct collision process with transfer of the full proton energy, but such simple events are relatively rare. In most cases there is a sequence involving incorporation of the bombarding proton into the nucleus, intra- and internuclear cascades accompanied by the ejection of assorted high-energy particles, including neutrons, and then an 'evaporation' process releasing neutrons from excited nuclei with

Table 2.3.3
Details on selected research reactors

The primary source of data is the IAEA Research Reactor Database (RRDB). The publicly accessible RRDB does not include information on fuel: limited information on this has been found from other internet sources.

Reactor (type)	Power (MW)	Location	Fuel (see text)	Moderator/ coolant	Reflector	Thermal flux (n cm^{-2} s^{-1})	Cold/hot neutron sources
CARR (tank in pool)	60	CIAE, Beijing, China	U_3Si_2-Al, LEU 19.75%	Light water	Heavy water	8×10^{14}	1 cold
FRM-II (pool)	20	TUM, Garching, Germany	U_3Si_2-Al, HEU	Light water	Heavy water	8×10^{14}	1 cold, 1 hot
HANARO (pool)	30	KAERI, Daejeon, Korea	U_3Si, LEU 19.75%	Light water	Heavy water	4.5×10^{14}	1 cold
HFIR (tank)	85	ORNL, Oak Ridge, USA	U_3O_8-Al, HEU 93%	Light water	Beryllium	2.5×10^{15}	1 cold
HFR (heavy water)	58.3	ILL, Grenoble, France	U_3Al_x-Al, HEU	Heavy water	Heavy water	1.5×10^{15}	2 cold, 1 hot
JRR-3M† (pool)	20	JAEA, Tokai, Japan	U_3O_8-Al, U_3Si_2-Al, LEU	Light water	Light water, heavy water, beryllium	2.7×10^{14}	1 cold
NBSR (heavy water)	20	NIST, Gaithersburg, USA	U_3O_8-Al HEU 93%	Heavy water	Heavy water	4×10^{14}	1 cold
OPAL (pool)	20	ANSTO, Sydney, Australia	U_3Si_2-Al, LEU 19.75%	Light water	Heavy water	2×10^{14}	1 cold

† This reactor has been temporarily shut down.

energies comparable to those released in the fission process (Carpenter, 1977; Carlile, 2003; Arai & Crawford, 2009). The numbers of neutrons released in these various processes depend on the proton energies and the target materials employed; for 1 GeV protons on a Pb target, around 25 neutrons are released per bombarding proton (Arai & Crawford, 2009). Target materials in use include Hg, Pb, W, Ta and ^{238}U (depleted uranium). The yield of neutrons per proton for non-fissionable target materials is approximated by $0.1(E - 0.12)(A + 20)$ where E is the proton energy in GeV and A is the atomic number of the target nucleus; for a target such as ^{238}U that is fissionable under bombardment by high-energy neutrons the yield is almost double that. Generally, the energy to be dissipated as heat in the spallation process will be no more than the energy of the bombarding proton, so for the example of 1 GeV protons on Pb it should not exceed 40 MeV per neutron produced. Nevertheless, cooling requires attention. The use of liquid targets such as Hg, and Pb either in pure form or in a Pb-Bi eutectic alloy, facilitates the dissipation of heat. Solid targets are usually water cooled. The fast neutrons from spallation need to be moderated, not in this case for sustaining the process, but simply to make them useful for diffraction and other applications. Moderators in common use include water, heavy water, liquid or solid methane (CH_4), and liquid hydrogen (H_2). The volumes of moderator are usually small, for reasons that will be explained below.

Most spallation neutron sources, though by no means all, operate in 'short-pulse mode', then employ time-of-flight methods in their instrumentation. The duration of the neutron pulse is critical in determining the time-of-flight resolution. Short-pulse operation depends first of all on a short-pulse structure of the bombarding protons. This is inherent in proton-accelerating systems that incorporate synchrotron accelerators or accumulator rings, since the protons become bunched[10] while travelling around these rings, and pulses of duration <1 μs are delivered. The frequency of these pulses is modest, say 50 Hz, in part to reduce power requirements, but also to avoid the situation in which the desired thermal (or cold) neutrons from one pulse are overtaken by fast neutrons from the next. For short-pulse operation, the proton pulse must be translated into a still-short pulse of moderated neutrons; this has significant implications for moderator design (Tamura *et al.*, 2003; Arai, 2008; Arai & Crawford, 2009; Batkov *et al.*, 2013; Zhao *et al.*, 2013; Thomsen, 2014). The normal processes of moderation – neutrons giving up energy in collisions with nuclei in the moderator until thermal equilibrium is achieved – need to be to some extent curtailed. One means to curtail these processes is to use only a small volume of moderator, so neutrons escape before spending excessive time in it. Another is to place neutron absorbers – cadmium or gadolinium – around the moderator, or indeed incorporate these absorbing materials into it, so that the slow neutrons remaining in the moderator are absorbed before the pulse length becomes excessive; in this case the moderator is said to be 'decoupled' from the target. For cold-neutron moderators on short-pulse spallation sources the use of an ambient-temperature 'pre-moderator' may be advantageous. Whatever the means to limit the dwell time in the moderator, the emerging neutrons will be under-moderated, hence their spectrum will contain more epithermal neutrons (*i.e.* neutrons with energies of the order of eV to keV) than fully moderated neutrons from a continuous source. Fig. 2.3.8 shows the results for energy spectra and pulse length, from Monte Carlo calculations, for different cryogenic moderators for the J-PARC spallation neutron source, Tokai, Japan. The neutron dwell time and therefore the pulse length are calculated to be smaller in the decoupled moderators (Fig. 2.3.8*b*), but comparison with the coupled moderator (Fig. 2.3.8*a*) shows that intensity is sacrificed. The pulse length in the high-energy region, and at lower energies for the poisoned moderators, varies as roughly $1/(E)^{1/2}$; from equation (2.3.1) this makes the pulse length Δt proportional to the wavelength λ. In a time-of-flight analysis we measure the flight time t over a length L; noting that $v = L/t$ and using that same equation we find that t is also proportional to λ, *viz.* $t = (mL/h)\lambda$. The result is that the time resolution $\Delta t/t$

[10] At the ISIS spallation neutron source, for example, the protons are injected into the synchrotron in 200 μs bursts, where they form two bunches each only 100 ns wide (detail from https://www.isis.stfc.ac.uk/Pages/How-ISIS-works–in-depth.aspx).

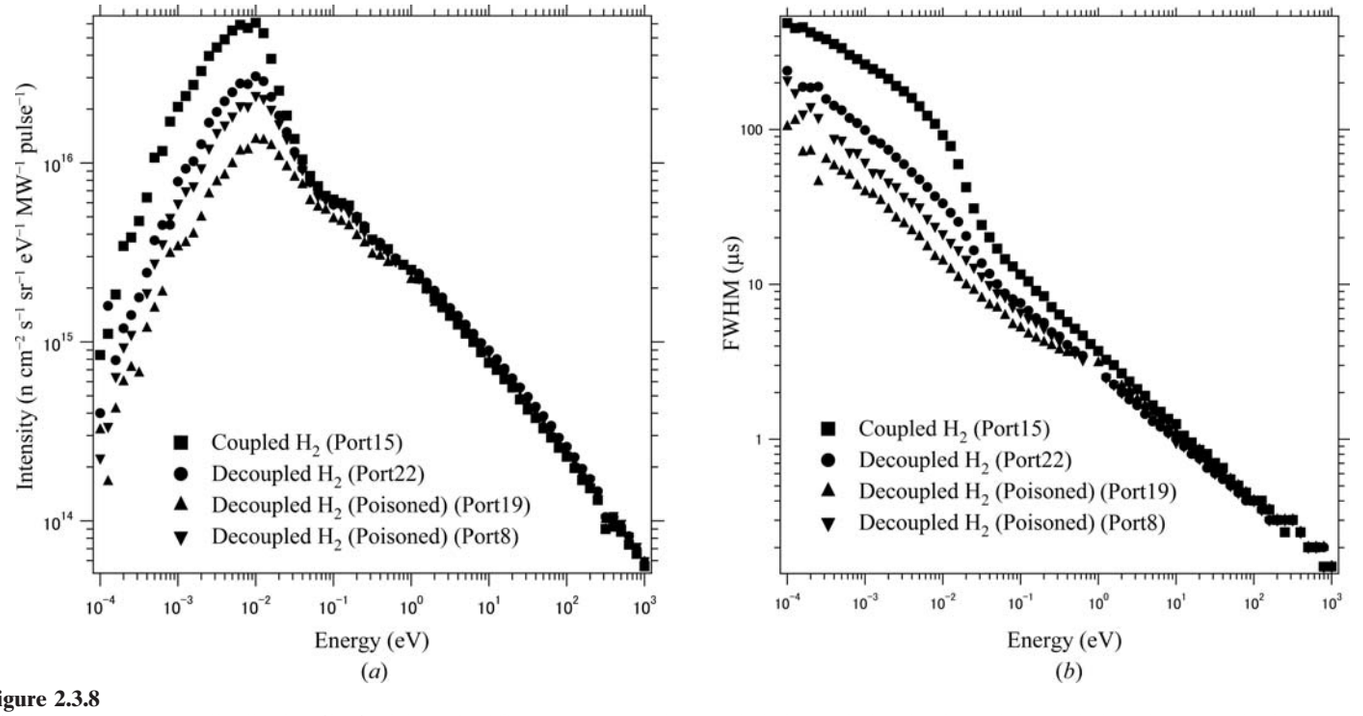

Figure 2.3.8
(*a*) The neutron energy distribution (flux) of the J-PARC neutron source for coupled, decoupled and poisoned decoupled moderators. The flux consists of a Maxwell distribution at low energies and a $1/E$ region at higher energies. (*b*) Pulse duration as a function of energy calculated for the same moderators. For the decoupled moderators, the peak widths vary approximately as $1/E^{1/2}$. Reproduced from Tamura *et al.* (2003).

is independent of flight time (or wavelength), which is a very satisfactory state of affairs (see Section 2.3.4.2.1).

As mentioned earlier, there is the problem for time-of-flight analysis that the slower neutrons from one pulse might be overtaken by the first arrivals from the next – a problem known as 'frame overlap'. Taking the example of 25 meV thermal neutrons, at a speed of 2190 m s^{-1} and a 50 Hz pulse repetition frequency, the neutrons from one pulse will have travelled 44 m when the next pulse occurs. If instrument flight paths are longer than this, or indeed if slower neutrons are involved, then the frame-overlap problem is encountered. A conceptually simple approach is to reduce the pulse frequency, and this has been implemented at the UK's ISIS neutron facility where Target Station 2 takes just one pulse in five from the proton-acceleration system, reducing the effective pulse frequency to 10 Hz; the other four pulses are directed to Target Station 1. Neutron choppers provide an alternative means to address this problem. The simplest kind of chopper is a disc (Fig. 2.3.9), usually of aluminium, nickel alloy or carbon fibre, coated in part with neutron-absorbing material such as boron, cadmium or gadolinium, rotating in a synchronous relationship with the source. A chopper located near to the source can be adjusted to block the fast neutrons and γ-rays that emerge immediately, but allow through neutrons in a restricted time window, from T_0 to $T_0 + \Delta T$, measured from the time of the pulse. Evidently, time $T_0 + \Delta T$ cannot exceed the time for a single rotation of the disc; when the disc is rotating at the pulse-repetition frequency this is the time between pulses. If the disc-rotation frequency is a submultiple of the pulse frequency, *i.e.* the rotation frequency is the pulse frequency divided by n, then the time window ΔT can be set to select only every nth pulse from the source. A two-chopper arrangement is used, for example, in the 96 m flight path of the High Resolution Powder Diffractometer (HRPD) at the ISIS facility; the first chopper at 6 m from the source runs at the pulse frequency and the second at 9 m from the source runs at one-fifth or one-tenth of that frequency, so that only every fifth or tenth pulse is used (HRPD user manual, http://www.isis.stfc.ac.uk/Pages/hrpd-manual.pdf).

Figure 2.3.9
One of the disc choppers in use at the ISIS neutron facility. This is an aluminium (2014A) alloy disc, and the neutron-absorbing coating (the darker region) is boron carbide in a resin. The cut-out on the right-hand side provides the aperture for neutrons. (Credit: STFC.)

Although we have introduced neutron choppers in the context of spallation sources, we should acknowledge that mechanical choppers and velocity selectors have a long history, dating back long before the advent of spallation sources. In fact, the first report on a velocity selector (Dunning *et al.*, 1935) pre-dates even the earliest demonstrations of neutron diffraction. Mechanical systems have long been used at continuous neutron sources to act as velocity (wavelength) selectors, and/or to tailor pulses of neutrons suitable for time-of-flight studies. Two disc choppers can be arranged to serve both purposes – the first chopper has a limited aperture transmitting a short pulse of neutrons, and the second chopper, with a similar aperture and located at some distance from the first, is phased so as to allow through only those neutrons with a particular velocity. This arrangement can provide short pulses of more-or-less monochromatic neutrons to an experiment. The helical velocity selector (Friedrich *et al.*, 1989) is conceptually somewhat similar. This takes the form of a cylinder,

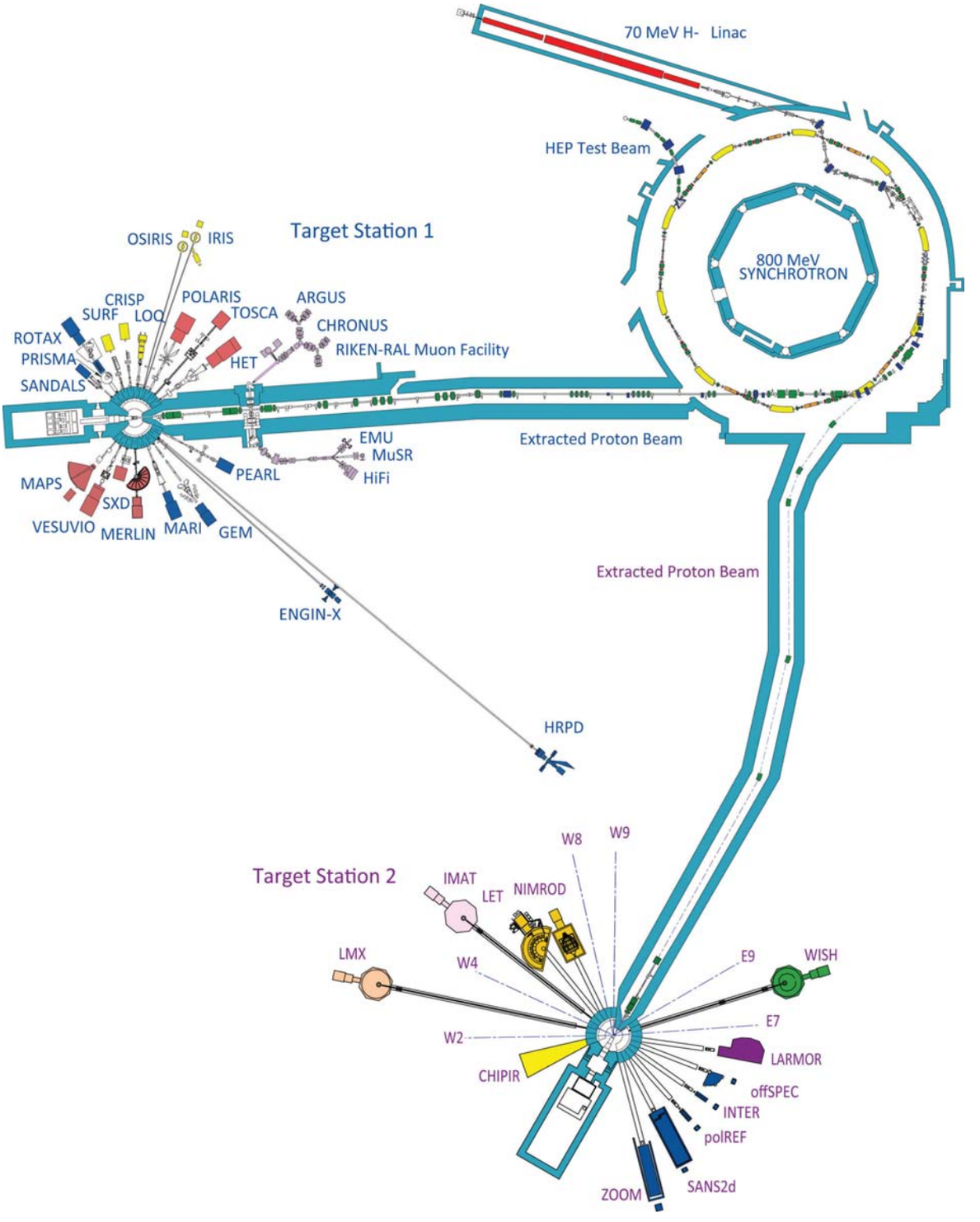

Figure 2.3.10
Layout of the ISIS spallation neutron source. (Credit: STFC.)

or indeed a stack of discs, rotating around an axis parallel to the neutron beam, with helical slits such that exits are offset from the entrance apertures in much the same manner as described above; the difference from the two-chopper arrangement is that there are apertures located all around the cylinder, giving closely spaced pulses unsuitable for time-of-flight studies. The purpose of mechanical wavelength selection at a continuous source is to select longer wavelengths and a broader range of wavelengths than a crystal monochromator (Section 2.3.4.1.2) could provide. Also worthy of mention is the Fermi chopper (Fermi *et al.*, 1947), comprising a package of neutron-transmitting slits set into a cylinder that rotates at rates of some hundreds of hertz around an axis in the plane of the slits, coincident with the cylinder axis, and perpendicular to the neutron beam. Neutrons above a threshold velocity are transmitted for the brief periods in which the slits are suitably aligned, so short (μs) but frequent pulses of neutrons are delivered. In a variation of the Fermi chopper (Marseguerra & Pauli, 1959), the transmitting slits are curved, providing for the transmission of rather slower neutrons while preventing the transmission of faster ones; in this variant the chopper not only delivers short pulses of neutrons but acts as a velocity selector as well. Neutron choppers are used in various combinations at both continuous and pulsed neutron sources; the Fermi chopper in particular can be used for 'shaping'

the pulses at long-pulse spallation neutron sources (Peters *et al.*, 2006).

As an initial case study, we consider the ISIS neutron facility, located in Oxfordshire, England, at the Rutherford Appleton Laboratory. This is a well established neutron spallation source supporting a strong programme of research using neutron beams. Of particular note are the excellent facilities for powder diffraction. First neutrons were delivered in 1984, but there have been upgrades since then, including the commissioning of a second target station in 2009. Fig. 2.3.10 is a schematic showing the layout of this facility. Some details about its operation are available on the ISIS web site, at https://www.isis.stfc.ac.uk/Pages/How-ISIS-works.aspx. Briefly, an ion source and radio-frequency quadrupole accelerator (not shown) inject bunches of negative hydrogen ions, H^-, into the linear accelerator where they are accelerated to 70 MeV. These are passed through aluminium foil, which strips them of their electrons, so they become protons, H^+, which are then accelerated to 800 MeV in the proton synchrotron. The protons, then travelling in two 100 ns bunches 230 ns apart, are kicked out of their synchrotron orbits and directed toward the targets. The whole process is repeated at a frequency of 50 Hz; the kickers are arranged to send one pulse in five to Target Station 2 (so that the pulse frequency there is just 10 Hz), and the remainder to Target Station 1. Both targets are made of tantalum-coated tungsten, as a stack of water-cooled plates in Target Station 1 and as a heavy-water surface-cooled cylinder in Target Station 2. As explained earlier, the fast neutrons produced in the spallation process must be moderated, and for this purpose moderators are located adjacent to the targets: two water moderators at 300 K, one liquid-methane moderator at 100 K and one liquid-hydrogen moderator at 20 K at Target Station 1; and one decoupled solid-methane moderator at 26 K and one coupled liquid-hydrogen/methane moderator at 26 K at Target Station 2. The widths of the pulses of the moderated neutrons are typically 30–50 μs, but 300 μs for the coupled moderator at Target Station 2. The target/moderator assemblies are surrounded, apart from beam exit ports, by beryllium reflectors. The schematic of Fig. 2.3.10 indicates the placement of the various neutron-beam instruments around the target stations.

The Swiss neutron spallation source, SINQ, located at the Paul Scherrer Institute in Villigen, is the only spallation source operating in continuous mode. SINQ reached full power in 1997. Since there is no time structure to be preserved, more generous quantities of moderator can be used; in fact the target, which becomes the source of neutrons, is located centrally in a moderator tank. The situation here is not very different from that in a medium-flux research reactor. The target comprises lead rods in Zircaloy tubes, the moderator is heavy water and there is a light-water reflector outside the moderator tank. Protons accelerated first by a Cockroft–Walton accelerator, then to 72 MeV by an injector cyclotron, and finally to 590 MeV in a proton ring cyclotron are directed onto the target from below (Fig. 2.3.11). The proton current is initially 2.4 mA, but this is reduced in muon production, so that only about 1.65 mA reaches the spallation target. The power is thus close to 1.0 MW. A horizontal insert in the moderator tank houses a liquid-deuterium cold source at 25 K.

As a final example we describe the 5 MW long-pulse European Spallation Source, now under construction in Lund, Sweden (see Fig. 2.3.12). A more detailed description is available at the ESS web site, https://europeanspallationsource.se/technology. The proton-acceleration system, although comprising a number of different components, will be linear. The protons from the ion source will be accelerated through a radio-frequency quadrupole and drift tube LINAC up to 90 MeV, then through a series of superconducting cavities up to the final energy of 2 GeV. This system will deliver proton pulses of 2.86 ms duration at a 14 Hz repetition rate; the average current will be 6.26 mA and hence the total power 5 MW. The target material will be helium-cooled tungsten encased in stainless steel, in the form of a 2.5 m-diameter rotating wheel. Such an arrangement assists in dissipation of the heat deposited in the target. Coupled liquid-hydrogen moderators will be located above and below the rotating wheel, and this assembly will be partially surrounded by a water pre-moderator and beryllium reflector. Neutron choppers will be used to shape the neutron pulses as required, and neutron optical systems will deliver neutrons to the experiments. First beam on target is expected in 2019.

Characteristics of these and other neutron spallation sources are recorded in Table 2.3.4. The information included there has been taken from the respective facility web sites.

2.3.3.4. *Neutron beam tubes and guides*

Ideally, neutron diffractometers should be designed following a holistic approach, designing the source of moderated neutrons, through the delivery system, to the instrument itself. This is not often possible in practice; for example the source must often be taken as a given, and in some cases the delivery of the neutrons as well. The holistic approach is commonly a very large Monte Carlo simulation, not suitable for purposes of description; in this chapter, therefore, we provide separate descriptions of these different components.

The simplest delivery system is a neutron beam tube or collimator. A collimator could comprise just two pinholes of diameters a_1 and a_2 cut into neutron-absorbing material, and placed at a distance L apart; this limits the divergence of the beam to (full angle) $2\alpha = (a_1 + a_2)/L$. It is of course possible to use apertures of different cross section, for example rectangular slits, if the divergence must be smaller in one direction than another.

Neutron guides are now widely used at both reactor and spallation neutron sources. These are able to transport neutrons over distances ranging to 100 m or more. They are evacuated tubes, normally of rectangular cross section, and transmission depends on the reflection of glancing-angle neutrons from the walls of the guide. The guides are constructed from glass plates with a reflective coating deposited on the internal surfaces.

Initially, total external reflection (Section 2.3.2.3) provided the basis for reflection; the coating was nickel, or preferably ^{58}Ni. Given that nickel has a face-centred cubic structure (4 atoms per unit cell) with lattice parameter 3.524 Å, and taking the scattering lengths from Table 2.3.2, we find from equation (2.3.6) that the critical glancing angles per unit wavelength for total external reflection are 0.10° Å^{-1} and 0.12° Å^{-1} for nickel and ^{58}Ni, respectively. Taking wavelengths of 0.4, 1.2 and 5 Å as representative of hot, thermal and cold neutrons, respectively (*cf.* Fig. 2.3.5), these angles for a nickel mirror are just 0.04, 0.12 and 0.5°. Consequently, these guides are most useful for transmitting cold neutrons and are moderately useful for thermal neutrons, but are not used for hot neutrons. The small glancing angles are demanding, not only on the precision of manufacture, but also because it is highly desirable to use a curved guide tube so there is no direct line of sight to the source (as in Fig. 2.3.13); this is a way of preventing fast neutrons and γ-radiation from impacting on the experiment. The guide tube still transmits a range of wave-

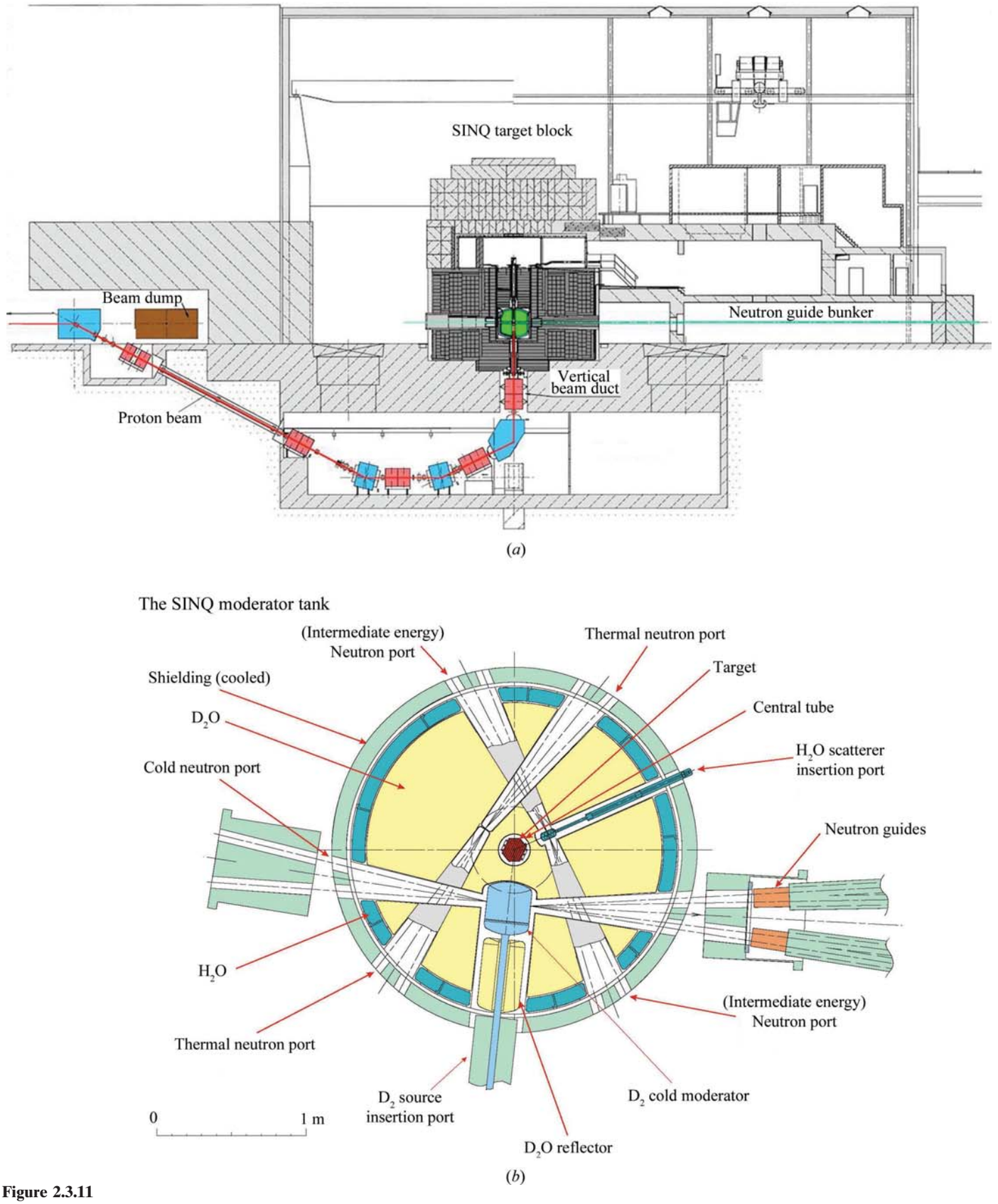

Figure 2.3.11
Layout at the SINQ neutron source. (*a*) Elevation: the target is located in the moderator tank, the high-energy protons being delivered from below. (*b*) Plan: showing the location of guide tubes relative to this central target. (Courtesy: Dr Bertrand Blau, Paul Scherrer Insitut.)

lengths, although only the longest wavelengths can travel by the zig-zag path indicated in Fig. 2.3.13. If the guide width is a, and its radius of curvature ρ (see Fig. 2.3.13), then the minimum length to avoid direct transmission is $(8a\rho)^{1/2}$. Critical to the transmission of a guide tube is the angle θ^*, which is the minimum glancing angle of incidence onto the outer surface that permits subsequent reflection from the inner surface, and is given by $\theta^* = (2a/\rho)^{1/2}$. The shortest wavelength, then, that can be transmitted involving reflection from the inner surface is given by [*cf.* equation (2.3.6)]

Table 2.3.4
Details of selected spallation neutron sources

Source	Type	Location	Proton energy	Current	Average power	Target(s)	Repetition rate (Hz)	Moderator(s)
CSNS†	Short pulse	Institute of High Energy Physics, Guangdong, China	1.6 GeV	62.5 μA	100 kW	Tungsten	25	Water, 2 × liquid hydrogen
ESS†	Long pulse	European Spallation Source, Lund, Sweden	2 GeV	2.5 mA	5 MW	Tungsten wheel (helium cooled)	14	2 × Liquid hydrogen (pancake geometry)
ISIS	Short pulse	Rutherford Appleton Laboratory, Oxfordshire, UK	800 MeV	200 μA	160 kW	2 × Tungsten	50	2 × Water, liquid methane, liquid hydrogen
							10	Hydrogen/methane, solid methane at 26 K
JSNS‡	Short pulse	J-Parc Centre, Tokai-mura, Japan	3 GeV	333 μA	1 MW	Liquid mercury	25	Supercritical hydrogen
LANSCE	Long pulse	Los Alamos National Laboratory, Los Alamos, USA	800 MeV	125 μA	100 kW	Tungsten	20	Water, 2 × liquid hydrogen
SINQ	Continuous	Paul Scherrer Institute, Villigen, Switzerland	590 MeV	1.64 mA§	0.97 MW	Lead	—	Heavy water; cold source: liquid deuterium at 20 K
SNS	Short pulse	Oak Ridge National Laboratory, Oak Ridge, USA	1 GeV	1.4 mA	1.4 MW	Liquid mercury	60	2 × Water, 2 × liquid hydrogen

† Under construction. ‡ Currently operating at <0.5 MW. § Current reaching spallation target after attenuation in muon source.

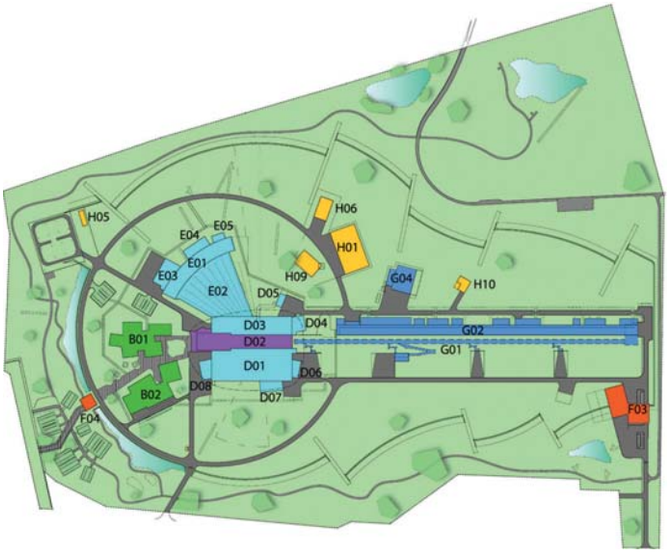

Figure 2.3.12
Schematic diagram of the ESS facility. The proton beam enters at the right, strikes the target and liberates neutrons for instruments in the three neutron experiment halls. (Image courtesy of the ESS.)

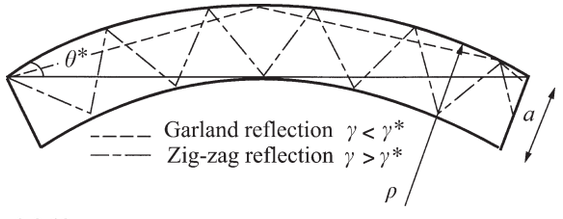

Figure 2.3.13
Plan of a curved neutron guide, indicating different possible neutron paths, labelled 'garland' and 'zig-zag'. Only the longer-wavelength neutrons can travel the zig-zag path because the glancing angles on this path (which must be less than the critical angle) are greater. In this schematic, the glancing angles, the width and the curvature have all been exaggerated. [From Section 4.4.2 of Volume C (Anderson & Schärpf, 2006).]

$$\lambda^* = \theta^* \left(\frac{\pi}{N b_{\rm coh}} \right)^{1/2}. \qquad (2.3.12)$$

This is known as the 'characteristic' wavelength of the guide [see Section 4.4.2 of Volume C by Anderson & Schärpf (2006)]; the majority of transmitted neutrons will have longer wavelengths than this.

The desire to use guides for shorter (*e.g.* thermal-neutron) wavelengths, and for retaining more neutrons at a given wavelength, has motivated the development of mirrors capable of reflecting neutrons incident at greater glancing angle. The earliest such mirrors were in fact monochromating mirrors obtained by laying down alternate layers of metals with contrasting coherent-scattering-length densities (Fig. 2.3.14). For a bilayer thickness d and angle of incidence θ these would select wavelengths according to Bragg's law [equation (1.1.3)],

$$\lambda = 2d \sin(\theta).$$

In an early implementation (Schoenborn *et al.*, 1974), the metals were Ge and Mn (which have coherent scattering lengths opposite in sign) and the bilayer thickness was of the order of 100 Å; this is a larger d-spacing giving access to longer wave-

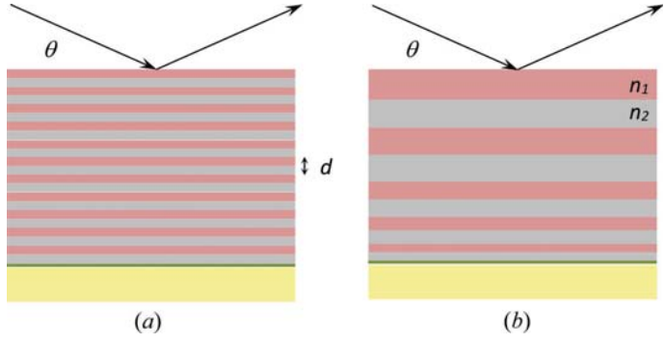

Figure 2.3.14
Schematic diagrams of (*a*) a multilayer monochromator and (*b*) a neutron supermirror.

lengths than would be accessible with the usual crystal monochromator (Section 2.3.4.1.2). The idea of supermirrors, comprising bilayers of graduated thickness, and in effect increasing the critical angle, was suggested by Turchin (1967) and Mezei (1976). For a perhaps simplistic explanation, we note first that since the bilayer dimension d is large compared with the neutron wavelength, we can approximate the above equation for reflection as

$$\theta \simeq \lambda \frac{1}{2d},$$

in which form it is reminiscent of equation (2.3.6). If we take $d_{\min}$ to be the thickness of the thinnest bilayer, then we can propose that the critical angle for reflection by the supermirror should be

$$\theta_c^{\rm SM} \simeq \lambda \frac{1}{2d_{\min}}. \qquad (2.3.13)$$

In order to ensure that all neutrons incident at angles less than this critical angle should be reflected, we need to incorporate a more-or-less continuous range of thicker bilayers into the supermirror (Fig. 2.3.14*b*). A more rigorous treatment (Hayter & Mook, 1989; Masalovich, 2013) takes account of the transmission and reflection at each interface, and lays down a prescription as to how the thicknesses should be varied. The most common pairing for the bilayer is now Ni with Ti; the coherent scattering cross sections are of opposite sign (see Table 2.3.2). The performance of a supermirror is normally quoted as the ratio m of the critical angle for the supermirror, $\theta_c^{\rm SM}$, to that for natural nickel, $\theta_c^{\rm Ni}$; a high value for reflectivity is also important. Supermirrors to m of 2 or 3 are in quite common use, while now Ni/Ti supermirrors with m up to 7 are offered for purchase (Swiss Neutronics AG; see also Maruyama *et al.*, 2007).

Consideration is currently being given to the variation of the cross section of the guide along its length. There is some loss on reflection by supermirrors, so these studies aim to reduce the number of reflections involved in transmission along the guide. One suggestion (also attributable to Mezei, 1997) is to use a 'ballistic guide', in which neutrons from the source travel through a taper of widening cross section into a length of larger guide, then through a taper of narrowing cross section to restore the original cross section at the exit. This is said to reduce the number of reflections suffered by the neutron by a factor of $(w_0/w)^2$, where w_0 is the width at entrance and exit and w the larger width along the main part of the guide (Häse *et al.*, 2002). Such a guide has been installed and is operating successfully on the vertical cold source at the Institut Laue–Langevin (Abele *et al.*, 2006). An extension of this idea is based on the well known property of ellipses that a ray emanating from one focus is reflected (just one bounce) to pass through the other; so if the guide cross section could be varied to give a very long ellipse, a source of neutrons placed at one focus, and the target point at the other, then perhaps the neutrons could be transmitted along the guide with just a single reflection (Schanzer *et al.*, 2004; Rodriguez *et al.*, 2011). Accordingly a number of neutron facilities have installed elliptical guides, and indeed a number of neutron powder diffractometers now are located on elliptical guides; these include diffractometer POWTEX at FRM-II, the high-resolution diffractometers HRPD and WISH at ISIS, and Super-HRPD at JSNS. Computer simulation by Cussen *et al.* (2013), however, questions whether, given the practicalities of finite source sizes and the approximation of elliptical variation by a number of linear segments, the theoretical improvement is fully realized.

2.3.4. Diffractometers

Put simply, the diffracted neutron beams associated with the different d-spacings in the sample under study satisfy Bragg's law,

$$\lambda = 2d\sin(\theta). \qquad (2.3.14)$$

As always, λ is the wavelength of the incident neutrons, and these neutrons are scattered through an angle 2θ.

There are basically two ways of exploiting this relationship. The first is to use a single wavelength for the investigation, in which case diffracted neutrons are observed at different angles 2θ corresponding to different d-spacings in the sample. A neutron powder diffractometer designed to carry out an investigation by this means we choose to call a 'constant wavelength' (CW) diffractometer. The other means is to fix the angle 2θ, illuminate the specimen with a range of wavelengths, and note the different wavelengths that are diffracted. In this case, we determine the wavelengths of the diffracted neutrons *via* their speed $\lambda = h/(mv)$ [equation (2.3.1)], and that in turn is measured by their flight time t over a path of length L, $v = L/t$; this leads to

$$\lambda = \frac{ht}{mL}. \qquad (2.3.15)$$

A diffractometer designed to carry out such an analysis of wavelengths we call a 'time-of-flight (TOF) diffractometer'.

The distinction between these two modes of operation can also be indicated *via* the Ewald construction in reciprocal space (Section 1.1.2.4). In this, the ideal powder is represented by concentric spheres in reciprocal space. In the constant-wavelength situation, the primary beam is fixed in direction and the Ewald sphere has a fixed radius; diffracted (reflected) beams are observed at any angle at which the surface of the Ewald sphere intersects one of the concentric spheres mentioned just above. In the wavelength-analysis (time-of-flight) situation, the directions of the primary and diffracted beams are fixed, but the radius of the Ewald sphere ($1/\lambda$) is variable through a range; diffracted beams are observed whenever the wavelength is such that the tip of the vector representing the reflected beam lies on one of the concentric spheres.

2.3.4.1. *Constant-wavelength neutron diffractometers*

The salient features of a constant-wavelength diffractometer are perhaps most easily explained by reference to a particular example; for this purpose we consider the High Resolution Powder diffractometer for Thermal neutrons (HRPT) installed at the SINQ continuous spallation source (Fischer *et al.*, 2000). Neutrons from the source travel through a guide tube to the crystal monochromator, which directs neutrons of a selected wavelength toward the sample. The diffracted neutrons are registered in a detector or detectors that cover a range of angles of scattering from the sample. Collimation is used to better define the directions of the neutron beams; in this instance a primary collimator is included in the guide tube and additional collimation is included between the sample and the position-sensitive detector. The various components will be described in more detail below.

2.3.4.1.1. *Collimation*

There need to be restrictions on the angular divergences of the neutron beams. The divergence of the beam impinging upon the crystal monochromator must be limited to better define the wavelength of the neutrons directed to the sample, whereas the divergences of the beams incident upon and diffracted from